

Observation of the electric Breit-Rabi Effect

S.-Z. Wang,^{1,*} S.-B. Wang,^{1,*} Z.-J. Tao,¹ T. Xia,^{2,†} and Z.-T. Lu^{1,2,‡}

¹*Hefei National Research Center for Physical Sciences at the Microscale,*

School of Physical Sciences, University of Science and Technology of China, Hefei 230026, China

²*Hefei National Laboratory, University of Science and Technology of China, Hefei 230088, China*

(Dated: July 14, 2025)

The response of an atom to external electric and magnetic fields can reveal fundamental atomic properties. It has long been verified that, in a static magnetic field, those atomic energy levels with hyperfine interactions shift according to the Breit-Rabi formula, which introduces nonlinear dependence on the magnetic field. On the other hand, the corresponding Breit-Rabi dependence on a static electric field has not been observed before due to a combination of experimental challenges. Here we precisely measure the Stark shift of the $6s^2\ ^1S_0 \leftrightarrow 6s6p\ ^1P_1$ transition of ^{171}Yb ($I = 1/2$) with cold atoms held by an optical dipole trap in a static electric field up to 120 kV/cm. We observe the electric Breit-Rabi effect displaying high-order (E^4 and E^6) DC Stark shifts. These effects arise from the influence of the strong electric field on hyperfine interactions.

I. INTRODUCTION

Extensive research has been conducted on the atomic Zeeman and Stark effects since both effects were discovered over a century ago [1, 2]. These effects are sensitive probes of fundamental atomic structure properties. They are also useful, and, indeed, are widely applied to control energy level shifts. For an atomic level with hyperfine interaction, its shift under the influence of an external DC magnetic field is described by the Breit-Rabi formula [3], which leads to approximately linear dependences on the magnetic field in both the weak-field Zeeman effect and the strong-field Paschen-Back effect [4]. In the intermediate-field region, where the energy shift is comparable to the hyperfine splitting, the dependence clearly deviates from linearity [5–7]. These dependencies have been accurately measured, and the Breit-Rabi formula confirmed, over a wide range of magnetic fields.

For an atomic level with hyperfine interaction, its Stark shift is expected to exhibit an electric-field version of the Breit-Rabi effect. In the intermediate-field region, the energy shift is predicted to deviate from its usual proportionality to the square of the electric field (E^2). The electric Breit-Rabi effect has appeared in textbooks [8] and theoretical calculations [9, 10], and has been applied to determine level-crossing points, which in turn led to hyperfine structure constants of high-lying excited states [11, 12]. However, the electric Breit-Rabi effect has never been verified with experimental measurements due to a combination of technical challenges. In this work, by precisely measuring the DC Stark shift of a transition in the ytterbium atom, we observe the electric Breit-Rabi effect displaying high-order (E^4 and E^6) dependences, thus establishing experimental validation of a fundamental atomic effect. Atoms in a laser field also exhibit Stark effects beyond the E^2 dependence [13, 14], known as hyperpolarizability, which arises from the 4th-order perturbation in the calculation without altering hyperfine interaction. In contrast, the electric Breit-Rabi effect originates from the coupling between the traditional Stark effect and hyperfine interaction. As shown in this work, at the 2nd-order perturbation level, the effect already exhibits high-order dependencies (E^4 and E^6).

The neutral ytterbium (Yb) atom possesses a rich Group-II-like energy level structure, providing long-lived clock states, long coherence times for the nuclear spin states, and transitions suitable for laser cooling and trapping. These characteristics combine to make Yb a favorite choice for a wide range of research, including optical clocks [15], quantum computation [16–18], Bose-Einstein condensation and Fermionic degenerate gases [19, 20]. The Stark effect often plays a crucial role in these works, for example, in evaluating the systematic error of an atomic clock due to blackbody radiation [21, 22], in realizing electric Feshbach resonances [23, 24], and in spin-state manipulation [25].

In this work, we measure the Stark shift of the $6s^2\ ^1S_0 \leftrightarrow 6s6p\ ^1P_1$ transition in ^{171}Yb (nuclear spin $I = 1/2$) atoms held by an optical dipole trap. The $6s6p\ ^1P_1$ energy level has a relatively small hyperfine splitting of 318 MHz [26]. As a result, when the electric field is in the practically reachable range of 30 - 100 kV/cm, the Stark interaction of this level is said to enter the intermediate-field region as its tensor energy shift, on the order of 20 - 200 MHz, becomes comparable to the hyperfine splitting. Using cold atoms for this measurement offers multiple advantages: the sample is of pure ^{171}Yb isotope; the sample fits through a small gap between electrodes so that a high electric field

* These authors contributed equally to this work.

† Corresponding author: txia@hfnl.cn

‡ Corresponding author: ztlu@ustc.edu.cn

can be applied; Doppler broadening is reduced, and systematic errors induced by quantum interference suppressed. Together, these advantages lead to improved measurement precisions.

II. ELECTRIC BREIT-RABI FORMULA

The Hamiltonian for Stark interaction can be expressed in the I - J coupled basis as [8, 10]

$$\langle F'm'_F | H_S | F''m''_F \rangle = -\frac{1}{2} (\alpha_s \mathcal{I} + \alpha_t \mathcal{Q}) E^2, \quad (1)$$

where E is the static electric field, its direction defined as the quantization axis. The scalar shift led by the static scalar polarizability (α_s) is the same for all hyperfine states, and $\mathcal{I} = \delta_{F'F''} \delta_{m'_F m''_F}$. On the other hand, the tensor shift (with α_t) varies due to hyperfine mixing and is described by the matrix element

$$\mathcal{Q} = \sqrt{\frac{(J'+1)(2J'+1)(2J'+3)(2F'+1)(2F''+1)}{J'(2J'-1)}} \times (-1)^{I+J'-m'_F} \begin{Bmatrix} F' & 2 & F'' \\ J' & I & J' \end{Bmatrix} \begin{pmatrix} F' & 2 & F'' \\ m'_F & 0 & -m''_F \end{pmatrix} \delta_{m'_F m''_F}. \quad (2)$$

By diagonalizing the Hamiltonian $H = A_{\text{hfs}} \mathbf{I} \cdot \mathbf{J} + H_S$, including both the hyperfine and Stark interaction, we obtain differential DC Stark shifts for the $6s^2 \ ^1S_0 \ |Fm_F\rangle \leftrightarrow 6s6p \ ^1P_1 \ |F'm'_F\rangle$ transitions in ^{171}Yb :

$$\Delta\nu = K_{F',m'_F} E^2 + f_{F',m'_F}(E), \quad (3)$$

where K_{F',m'_F} represents the differential DC Stark shift rate (see SI Appendix). The first term in Eq. 3 describes the commonly known 2nd-order DC Stark shift, which arises from the mixing between energy levels of opposite parities, e.g. between S and P levels. The second term describes high-order Stark shifts that arise from state mixing between different hyperfine levels due to the action of the electric field on I - J coupling, and these mixings form superpositions of states with the same parity.

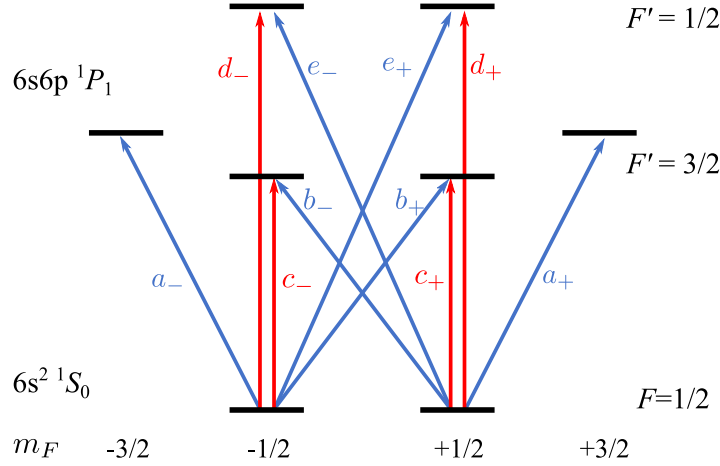


FIG. 1. Energy levels and transitions of ^{171}Yb . The $6s^2 \ ^1S_0 \leftrightarrow 6s6p \ ^1P_1$ transition has a wavelength of 399 nm and a natural linewidth $\Gamma = 2\pi \times 28.9$ MHz [27]. The hyperfine splitting between $F' = 1/2$ and $F' = 3/2$ of $6s6p \ ^1P_1$ is 318.5 MHz. π transitions (red) are labeled c_{\pm} and d_{\pm} ; σ transitions (blue) labeled a_{\pm} , b_{\pm} and e_{\pm} .

For the case of the E field pointing in the quantization axis, state mixing due to the tensor Stark interaction only occurs between states of the same m_F . In the $6s6p \ ^1P_1$ level of ^{171}Yb (Fig. 1), the high-order terms $f_{3/2,\pm 3/2}(E)$ equal to zero because there are no state mixing for the $^1P_1 \ |3/2, \pm 3/2\rangle$ states. On the other hand, the hyperfine states of $m_F = \pm 1/2$ experience state mixing under the tensor Stark effect, and the new energy eigenstates are superpositions of $^1P_1 \ |3/2, 1/2\rangle$ and $^1P_1 \ |1/2, 1/2\rangle$ (or $^1P_1 \ |3/2, -1/2\rangle$ and $^1P_1 \ |1/2, -1/2\rangle$). We derive an electric-field version of

the Breit-Rabi formula (see SI Appendix),

$$\begin{aligned} f_{F',m_F'}(E) &= \pm \frac{1}{4} \left(\alpha_t E^2 + 3A_{\text{hfs}} - 3A_{\text{hfs}} \sqrt{1 + \frac{2}{3}x + x^2} \right) \\ &= \pm \frac{A_{\text{hfs}}}{3} \left(-\frac{\alpha_t^2}{A_{\text{hfs}}^2} E^4 + \frac{\alpha_t^3}{3A_{\text{hfs}}^3} E^6 + \mathcal{O}\left(\frac{\alpha_t^4}{A_{\text{hfs}}^4} E^8\right) \right), \end{aligned} \quad (4)$$

where the symbol \pm correspond to the energy shifts of the upper and lower states. In analogy to the magnetic-field version, the unitless parameter $x = \alpha_t E^2 / A_{\text{hfs}}$ describes the size of the field effect relative to that of the hyperfine effect. In the weak-field case ($x \ll 1$), it is well known that the Stark shift is proportional to E^2 . However, in the intermediate-field region ($x \sim 1$), the term $f_{F',m_F'}(E)$ displays high-order Stark effects. In this study, we explore the region of $0 < x < 0.9$.

III. EXPERIMENTAL SETUP

^{171}Yb atoms are captured and cooled by a two-stage magneto-optical trap system. The cold atoms are transported to a neighboring science chamber with an optical dipole trap (ODT) for spectral measurement. Sample preparation, including atom trapping and transport, as well as high-voltage ramping, takes a total of approximately 20 s. As shown in Fig. 2, the ODT propagates along the x direction, and is linearly polarized along the z axis. Its wavelength of 1035.8 nm is set at the magic wavelength of the $6s^2\ ^1S_0 \leftrightarrow 6s6p\ ^3P_1$ transition [28]. With a power of 30 W, radius of 60 μm , and Rayleigh length of 7 mm, it achieves a trap depth of 100 μK . In the ODT, more than 1×10^6 atoms at 40 μK form a cloud of 100 μm size transversely and 8 mm longitudinally. At a vacuum pressure of approximately 1×10^{-11} torr, the trap lifetime of atoms in the ODT, positioned between the electrodes, is measured to exceed 70 s.

The atoms are positioned at the center between the electrodes. A uniform electric field is generated by a pair of parallel (tilt < 2 mrad) copper electrodes with a diameter of 16 mm and a separation distance measured optically to be 1.08(5) mm, which directly leads to a conversion factor between the voltage and the electric field to be 9.26(43) (kV/cm)/kV. Meanwhile, Stark shift measurements are performed to calibrate the same conversion factor, resulting in a more precise value of 8.654(14) (kV/cm)/kV. With a difference of 1.4 times the standard deviation, the two values are statistically consistent with each other, and are combined to produce a weighted average value of 8.655(14) (kV/cm)/kV. For this calibration, we measure the Stark shifts of the $6s^2\ ^1S_0 \leftrightarrow 6s6p\ ^3P_1$ transition of the ^{176}Yb isotope (nuclear spin $I = 0$, no hyperfine structure), and compare results with the published values from Li *et al.* [29] (see SI Appendix). In the work of Li *et al.*, measurements were carried out with an atomic beam through a pair of electrodes with a large spacing of 1.0163(3) cm, which was measured using machinist's gauge blocks [29].

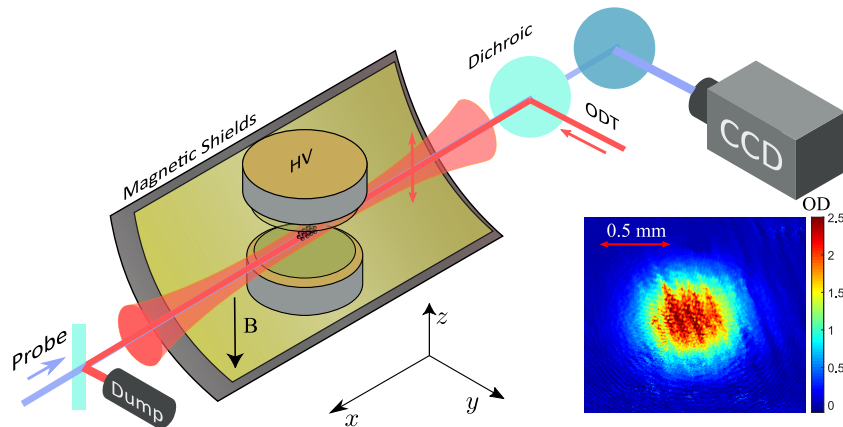


FIG. 2. Experimental setup. 1×10^6 ^{171}Yb atoms are trapped in the optical dipole trap (ODT). A pair of copper electrodes generate a static E field up to 120 kV/cm along z . A $\cos(\theta)$ coil inside the magnetic shields provides a bias B field of 20 mG, also along z . The probe laser beam propagates along x . The absorption image is captured using a CMOS camera, and the colorbar represents the optical density (OD). The figure is created using the open-source ComponentLibrary[30].

A probe laser at the wavelength of 399 nm is used to perform spectroscopy on the $6s^2\ ^1S_0 \leftrightarrow 6s6p\ ^1P_1$ transition and measure its Stark shifts. Combined with the ODT, the probe laser beam also propagates along the x -direction

(Fig. 2). The beam diameter of 2 cm is much larger than the size of the atom cloud so that its intensity on the atoms is approximately uniform at $50 \mu\text{W}/\text{cm}^2$ (to be compared to the saturation intensity of $58 \text{ mW}/\text{cm}^2$). A sideband generated by a fiber-EOM is frequency locked to a ULE cavity, and the carrier is used to scan across spectra as the EOM frequency is changed.

Fig. 1 illustrates the hyperfine structure of the $6s^2 \ ^1S_0 \leftrightarrow 6s6p \ ^1P_1$ transitions in ^{171}Yb , with each transition labelled by a letter from a_{\pm} to e_{\pm} . For certain measurements, the detection beam is set to be linearly polarized along z to induce π transitions labelled by c_{\pm} and d_{\pm} ; for other measurements, linear polarization along y is used to induce σ transitions labelled by a_{\pm} , b_{\pm} and e_{\pm} . The absorption signal is captured by a CMOS camera with an exposure time of 0.4 ms as shown in Fig. 2. The ODT is turned off at 2 ms before each camera exposure in order to avoid light shifts.

IV. SPECTROSCOPY

The interplay between hyperfine and Stark interactions not only induces energy shifts described by the electric Breit-Rabi formula, but also causes transition rates to vary. As the electric field increases, the eigenstates evolve from the pure I - J coupling states $|Fm_F\rangle$ to their superpositions $|\overline{Fm_F}\rangle$, leading to changes in transition rates. In particular, transitions b_{\pm} become more and more suppressed as the electric field increases. More details of the transition-rate measurements are provided in SI Appendix.

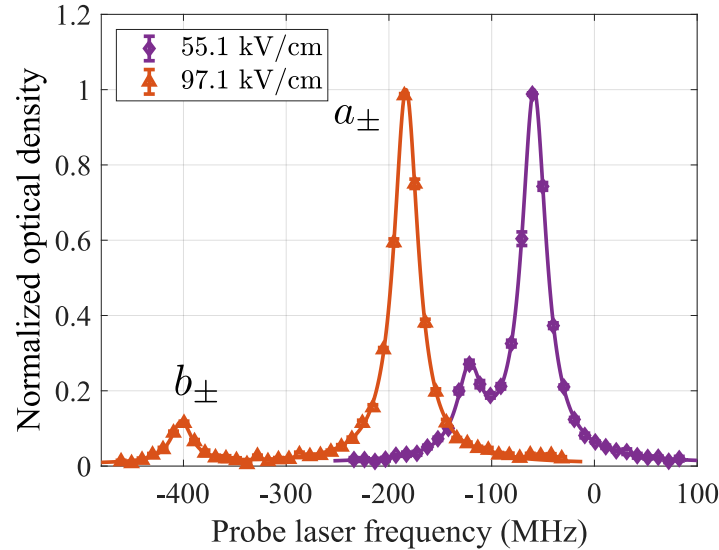


FIG. 3. The spectra of transitions a_{\pm} (higher peaks) and b_{\pm} (lower peaks) under the E field of 55.1 kV/cm (puple) and 97.1 kV/cm (red), respectively. The vertical axis represents the normalized optical depth, with each spectrum normalized independently.

Each absorption spectrum displayed in Fig. 3 contain two peaks: the higher peak on the right is due to transitions a_{\pm} , $^1S_0 \ |1/2, \pm 1/2\rangle \leftrightarrow ^1P_1 \ |3/2, \pm 3/2\rangle$, and lower peak on the left is due to transitions b_{\pm} , $^1S_0 \ |1/2, \pm 1/2\rangle \leftrightarrow ^1P_1 \ |3/2, \mp 1/2\rangle$. The frequency difference between the two peaks is the tensor Stark splitting, and the ratio between the two peak heights reflects the relative change of these transition rates.

At the bias magnetic field of 20 mG, the Zeeman shifts (~ 30 kHz) are much smaller than the natural linewidth. Moreover, because the Zeeman shifts of the $+m_F$ and $-m_F$ states are equal but with opposite signs, their combined effect only slightly broadens the spectra lines without shifting the peak positions.

V. HIGH-ORDER STARK SHIFTS

Fig. 4(a) displays the measured Stark shifts of $6s^2 \ ^1S_0 \leftrightarrow 6s6p \ ^1P_1$ in ^{171}Yb . The purple data points represent shifts of the transitions to the stretched states, $^1S_0 \ |1/2, \pm 1/2\rangle \leftrightarrow ^1P_1 \ |3/2, \pm 3/2\rangle$. Without high-order Stark shifts, their dependence on E^2 is linear with a fitted slope of $-19.43 \pm 0.01_{\text{stat}} \pm 0.06_{\text{sys}} \text{ kHz}/(\text{kV}/\text{cm})^2$. This result

is in agreement with, and more accurate by a factor of six than, the value of -19.82 (35) kHz/(kV/cm) 2 reported by Kawamura *et al.* [31]. The red and blue data points represent the Stark shifts of $^1S_0 |1/2, \pm 1/2\rangle \leftrightarrow ^1P_1 |3/2, \pm 1/2\rangle$ and $^1S_0 |1/2, \pm 1/2\rangle \leftrightarrow ^1P_1 |1/2, \mp 1/2\rangle$ transitions, respectively, both experiencing state mixing among hyperfine levels due to Stark interactions. By fitting the data in Fig. 4(a) with the function given in Eq. 3 and Eq. 12, the shifts can be attributed to two parts: the regular 2nd-order and the high-order Stark shifts. The red and blue dashed straight lines represent the frequency shifts caused solely by the 2nd-order Stark effect ($K_{F',m'_F} E^2$). The difference between the data points and the dashed straight lines, or the solid fit lines and the dashed straight lines, correspond to the high-order Stark shift $f_{F',m'_F}(E)$, and, for clarity, are plotted in Fig. 4(b). As shown clearly in Fig. 4(b), the electric Breit-Rabi formula (Eq. 12, blue and red lines) achieves a good agreement with data ranging from $x = 0$ to $x = 0.9$ at 100 kV/cm.

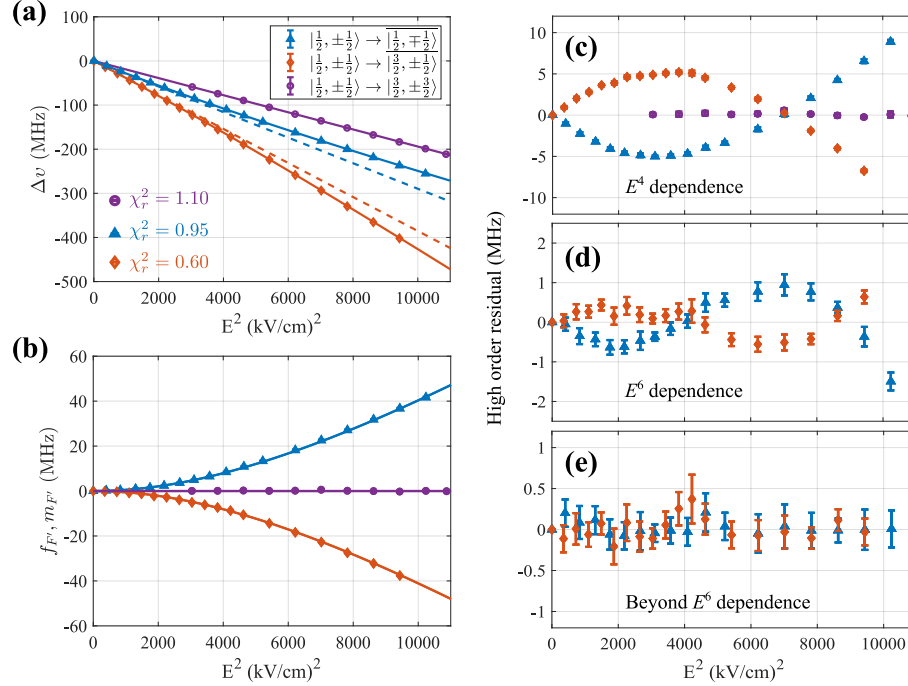


FIG. 4. Stark shifts vs. E^2 . (a) $\Delta\nu$ vs. E^2 . For clarity, the hyperfine shifts are removed, leaving only the Stark shifts. The error bars are smaller than the symbol size. The solid lines represent fitting by functions $\Delta\nu = K_{F',m'_F} E^2 + f_{F',m'_F}(E)$ given in Eq. 3. The red and blue dashed straight lines represent the frequency shifts caused solely by the 2nd-order Stark shifts, $K_{F',m'_F} E^2$. (b) $f_{F',m'_F}(E)$ vs. E^2 . The data points come from the difference between the data in Fig. (a) and the dashed straight lines; The solid lines represent fitting by functions $f_{F',m'_F}(E)$ given in Eq. 12. (c-e) Stark shift data are fit with polynomial functions instead of Eq. 3). (c) Residuals of fitting by the polynomial $\Delta\nu = \beta_2 E^2$. (d) Residuals of fitting by the polynomial $\Delta\nu = \beta_2 E^2 + \beta_4 E^4$. (e) Residuals of fitting by the polynomial $\Delta\nu = \beta_2 E^2 + \beta_4 E^4 + \beta_6 E^6$.

In order to demonstrate the unambiguous presence of high-order effects, the data in Fig. 4(a) are fitted with $\Delta\nu = \beta_2 E^2$. The resulting fit residuals appear as a quadratic polynomial of E^2 (Fig. 4(c)), thus demonstrating the presence of an E^4 dependence. Likewise, the data in Fig. 4(a) are fitted with $\Delta\nu = \beta_2 E^2 + \beta_4 E^4$. Its fit residuals form a cubic polynomial of E^2 (Fig. 4(d)), which clearly demonstrates the presence of an E^6 dependence. Only when data in Fig. 4(a) are fitted with $\Delta\nu = \beta_2 E^2 + \beta_4 E^4 + \beta_6 E^6$, the fit residue appears flat within error bars (Fig. 4(e)), thus suggesting that E^8 and higher -order terms are below the noise background. In conclusion, the electric-field version of the Breit-Rabi formula is verified in this work with experimental measurements.

Quantum interference between transitions of different hyperfine levels is commonly present in spectral measurements [32–34]. For example, in Kleinert *et al.* [26], the hyperfine structure constants of the $6s6p$ 1P_1 level in ^{171}Yb were determined using the fluorescence method, where a correction on the order of MHz due to quantum interference was made to obtain the final result of $A_{\text{hfs}} = -212.3(3)$ MHz. In this work, we record spectra by the absorption imaging method instead of fluorescence detection. Among other advantages, the absorption method effectively suppresses systematic errors of quantum interference [33]. We determine the hyperfine structure constant of the same energy level to be $A_{\text{hfs}} = -212.4(1)$ MHz. No correction of quantum interference is needed in this work.

Moreover, the high-order Stark shifts induced by the electric Breit-Rabi effect provides additional coefficients that

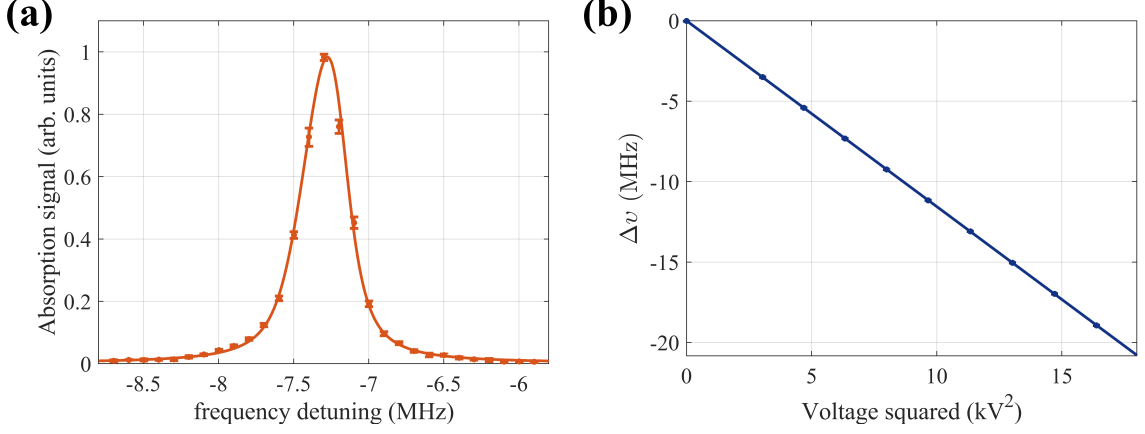


FIG. 5. Differential DC Stark shift rate of the $6s^2 \ ^1S_0 |0,0\rangle \leftrightarrow 6s6p \ ^3P_1 |1,0\rangle$ transition in the even isotope ^{176}Yb . (a) Spectrum at 2.516 kV, with a resonance frequency of -7.319(12) MHz and a FWHM of 300 kHz. The spectrum is fit with a modified Voigt lineshape, which considers the effect due to acceleration of the atoms by the probe beam. (b) The horizontal axis represents the square of the voltage, and the vertical axis represents the resonance frequency at different voltages. The slope obtained by linear fitting is -1154.7(7) kHz/kV². The error bars in the figure are from the statistical error of multiple measurements.

can be used to extract the scalar and tensor polarizability. By fitting the blue and red solid lines in Fig. 4(a) with Eq. 3, and with A_{hfs} given the above value, we obtain both the static tensor polarizability $\alpha_t = -19.35 \pm 0.08_{\text{stat}} \pm 0.06_{\text{syst}}$ kHz/(kV/cm)² and the differential static scalar polarizability $\Delta\alpha_s = \alpha_s(^1P_1) - \alpha_s(^1S_0) = 57.99 \pm 0.07_{\text{stat}} \pm 0.19_{\text{syst}}$ kHz/(kV/cm)² for the 1P_1 level of ^{171}Yb . The values are obtained independently by fitting either the $^1S_0 |1/2, \pm 1/2\rangle \leftrightarrow ^1P_1 |3/2, \pm 1/2\rangle$ or the $^1S_0 |1/2, \pm 1/2\rangle \leftrightarrow ^1P_1 |1/2, \mp 1/2\rangle$ transition, and are consistent with each other, as shown in SI Appendix. They also agree with the values obtained on even isotopes by Kawamura *et al.* [31], as the polarizability values are shared by all Yb isotopes.

VI. CONCLUSION

By measuring the DC Stark shifts of the $6s6p \ ^1P_1$ level in ^{171}Yb atoms, we have observed the electric Breit-Rabi effect for the first time. The Zeeman effect and the Stark effect are two fundamental effects that describe the interaction between atoms and external fields. While the full Zeeman effect has long been verified experimentally, the measurement of the electric Breit-Rabi effect in this work completes the experimental verification of the Stark effect.

The nonlinearity in the magnetic Breit-Rabi effect has been employed to achieve magic conditions at which the differential energy between some hyperfine or Zeeman states becomes insensitive to variation of magnetic field, leading to a longer qubit coherence time in $^{43}\text{Ca}^+$ [35] and a frequency standard based on $^9\text{Be}^+$ [36]. Likewise, the high-order part of the electric Breit-Rabi effect offers additional degrees of freedom for tuning atomic level shifts in order to achieve magic conditions for applications in quantum information processing and precision measurements.

VII. METHOD

To calibrate the electric field, we measure the DC Stark shift of the $6s^2 \ ^1S_0 \leftrightarrow 6s6p \ ^3P_1$ transition (wavelength 556 nm) of the even isotope ^{176}Yb ($I = 0$) and compare it with the differential DC Stark shift rate K given in Ref. [29], which is $K = -15.419(48)$ kHz/(kV/cm)². The detection light polarization (parallel to the electric field) and the atomic transition in our measurement are the same as those in Ref. [29]. The measurement results are shown in SI Appendix. By linear fitting, we obtain a slope of -1154.7(7) kHz/(kV²). From our measurement and the reference value, we obtain a conversion factor between the voltage applied and the resulting electric field of 8.654(14) (kV/cm)/kV. The error in this result mainly comes from the spectral measurement error in the Ref. [29].

The Breit-Rabi effect is observed by measuring the absorption spectra of the $6s^2 \ ^1S_0 \leftrightarrow 6s6p \ ^1P_1$ transition in ^{171}Yb . The probe laser with wavelength 399 nm can be frequency-scanned using a fiber-EOM. Additional details are described in SI Appendix.

Considering both the hyperfine interaction and the DC Stark interaction, we can obtain the energy level shifts of the hyperfine structure under an external electric field as well as the changes in the eigenstate. Additionally, the

presence of the static electric field induces state mixing between different hyperfine structures, leading to changes in the transition rates of electric dipole transitions. Additional details are described in the SI Appendix.

VIII. SUPPORTING INFORMATION

Considering only the hyperfine interaction, the eigenstate of ^{171}Yb is denoted as $|Fm_F\rangle$. The hyperfine interaction Hamiltonian H_{hfs} is given by

$$\langle F'm'_F | H_{\text{hfs}} | F''m''_F \rangle = \frac{A_{\text{hfs}}}{2} (F'(F'+1) - I(I+1) - J(J+1)) \delta_{F'F''} \delta_{m'_F m''_F},$$

where A_{hfs} is the magnetic dipole hyperfine constant, $F'(F'')$ is the total angular momentum quantum number, I is the nuclear spin, and J is the total electronic angular momentum. For ^{171}Yb , the nuclear spin $I = 1/2$, hence, the electric quadrupole moment is zero, and there is no electric quadrupole contribution to the hyperfine interaction.

The DC Stark interaction H_S in the presence of hyperfine structure is given by [8, 37, 38]

$$\langle F'm'_F | H_S | F''m''_F \rangle = -\frac{1}{2} (\alpha_s \mathcal{I} + \alpha_t \mathcal{Q}) E^2. \quad (5)$$

Considering both hyperfine interaction and DC Stark interaction, the total Hamiltonian is given by

$$H_{\text{tot}} = H_{\text{hfs}} + H_S. \quad (6)$$

The excited state $6s6p^1P_1$ level has two hyperfine structures, labeled as $F = 3/2$ and $F = 1/2$, with a total of six distinct Zeeman sublevels. By substituting the energy level structure into Eq. VII, Eq. 5 and Eq. 6, the matrix representation of H_{tot} is given by

$$\begin{pmatrix} |3/2, +3/2\rangle & |1/2, 1/2\rangle & |3/2, 1/2\rangle & |1/2, -1/2\rangle & |3/2, -1/2\rangle & |3/2, -3/2\rangle \\ \frac{A_{\text{hfs}} - (\alpha_s + \alpha_t)E^2}{2} & 0 & 0 & 0 & 0 & 0 \\ 0 & -A_{\text{hfs}} - \frac{\alpha_s E^2}{2} & \frac{\alpha_t E^2}{\sqrt{2}} & 0 & 0 & 0 \\ 0 & \frac{\alpha_t E^2}{\sqrt{2}} & \frac{A_{\text{hfs}} - (\alpha_s - \alpha_t)E^2}{2} & 0 & 0 & 0 \\ 0 & 0 & 0 & -A_{\text{hfs}} - \frac{\alpha_s E^2}{2} & -\frac{\alpha_t E^2}{\sqrt{2}} & 0 \\ 0 & 0 & 0 & -\frac{\alpha_t E^2}{\sqrt{2}} & \frac{A_{\text{hfs}} - (\alpha_s - \alpha_t)E^2}{2} & 0 \\ 0 & 0 & 0 & 0 & 0 & \frac{A_{\text{hfs}} - (\alpha_s + \alpha_t)E^2}{2} \end{pmatrix} \quad (7)$$

The matrix H_{tot} shows that the matrix contains non-zero off-diagonal elements when both hyperfine interaction and DC Stark interaction are considered. This indicates that the angular momentum eigenstates are mixed, which only occurs between Zeeman sublevels with the same m_F but different F . Specifically, mixing occurs between the hyperfine states $|3/2, 1/2\rangle$ and $|1/2, 1/2\rangle$, and between $|3/2, -1/2\rangle$ and $|1/2, -1/2\rangle$. However, in the stretched states where $m_F = \pm 3/2$, there are no pairs of Zeeman sublevels with the same m_F , so state mixing does not affect the stretched states. The energy eigenstates of H_{tot} are denoted as $|\overline{F}, m_F\rangle$. In the absence of an electric field, $|\overline{F}, m_F\rangle = |F, m_F\rangle$.

Diagonalizing H_{tot} yields the atom's eigenenergies and eigenstates under the combined influence of the static electric field and hyperfine interaction. The eigenenergies are given by

$$\begin{aligned} \mathcal{E}(|\overline{3/2}, \pm 3/2\rangle) &= \frac{A_{\text{hfs}} - (\alpha_s + \alpha_t)E^2}{2} \\ \mathcal{E}(|\overline{3/2}, \pm 1/2\rangle) &= -\frac{1}{2}\alpha_s E^2 + \frac{1}{4} \left(\alpha_t E^2 - A_{\text{hfs}} + 3A_{\text{hfs}} \sqrt{1 + \frac{2\alpha_t E^2}{3A_{\text{hfs}}} + \frac{\alpha_t^2 E^4}{A_{\text{hfs}}^2}} \right) \\ \mathcal{E}(|\overline{1/2}, \pm 1/2\rangle) &= -\frac{1}{2}\alpha_s E^2 + \frac{1}{4} \left(\alpha_t E^2 - A_{\text{hfs}} - 3A_{\text{hfs}} \sqrt{1 + \frac{2\alpha_t E^2}{3A_{\text{hfs}}} + \frac{\alpha_t^2 E^4}{A_{\text{hfs}}^2}} \right). \end{aligned} \quad (8)$$

Eq. 8 represents the energy shifts due to both the hyperfine interaction and the DC Stark effect. After subtracting the energy shifts due to the hyperfine interaction alone, the differential energy shift $\Delta\mathcal{E}_S$ between the excited state $|\overline{F'm'_F}\rangle$ and the ground state $|Fm_F\rangle$ caused solely by the static electric field is given by

$$\Delta\mathcal{E}_S(|\overline{F'm'_F}\rangle) = K_{F', m'_F} E^2 + f_{F', m'_F}(E), \quad (9)$$

where the ground state of ^{171}Yb is $6s^2\ ^1S_0$ with $F = \frac{1}{2}$. This level structure is simple and does not exhibit tensor Stark shifts related to F and m_F . Therefore, the differential energy shift presented in the equation is solely connected to the hyperfine structure of the excited state. The first term is linearly dependent on the square of the electric field (E^2) and arises from the state mixing between the electronic energy levels with opposite parities, e.g. between S and P states. The expression for the differential DC Stark shift rate K_{F',m'_F} is given by

$$\begin{aligned} K_{F',m'_F} &= -\frac{1}{2} \left(\alpha_s + \frac{3m_F'^2 - F'(F' + 1)}{F'(2F' - 1)} \alpha_t - \alpha_s^g \right) & F' > 1/2 \\ K_{F',m'_F} &= -\frac{1}{2} (\alpha_s - \alpha_s^g) & F' \leq 1/2, \end{aligned} \quad (10)$$

where α_s^g is the static scalar polarizability of the ground state. The second term in Eq. 9 is non-linearly dependent on E^2 and originates from the state mixing between different hyperfine states with same parity. The non-linear term represents the high-order Stark shifts and, by combining Eq. 9 and Eq. 10, we obtain the electric version of the Breit-Rabi formula

$$f_{F',m'_F}(E) = \pm \frac{1}{4} \left(\alpha_t E^2 + 3A_{\text{hfs}} - 3A_{\text{hfs}} \sqrt{1 + \frac{2}{3}x + x^2} \right), \quad (11)$$

where $x = \alpha_t E^2 / A_{\text{hfs}}$, and the symbol \pm correspond to the energy shifts of the upper and lower hyperfine states.

By diagonalizing the matrix H_{tot} we obtain not only the energy eigenvalues $\mathcal{E}(|F, m_F\rangle)$ but also the energy eigenstates $|\overline{F}, m_F\rangle$

$$\begin{aligned} |\overline{3/2, \pm 3/2}\rangle &= |3/2, \pm 3/2\rangle \\ |\overline{3/2, \pm 1/2}\rangle &= \sqrt{\frac{r + (1 + \frac{1}{3}x)}{2r}} |3/2, \pm 1/2\rangle \pm \text{sign}(x) \sqrt{\frac{r - (1 + \frac{1}{3}x)}{2r}} |1/2, \pm 1/2\rangle \\ |\overline{1/2, \pm 1/2}\rangle &= \sqrt{\frac{r + (1 + \frac{1}{3}x)}{2r}} |1/2, \pm 1/2\rangle \mp \text{sign}(x) \sqrt{\frac{r - (1 + \frac{1}{3}x)}{2r}} |3/2, \pm 1/2\rangle, \end{aligned} \quad (12)$$

where $r(x) = \sqrt{1 + \frac{2}{3}x + x^2}$ and $\text{sign}(x)$ is the sign function. For ^{171}Yb in the $6s6p\ ^1P_1$ state, $\alpha_t < 0$ and $A_{\text{hfs}} < 0$, hence $\text{sign}(x) = 1$. This condition is used throughout this material. Eq. 12 also indicates that in the presence of an electric field, state mixing occurs between Zeeman sublevels with the same m_F but different F , resulting in F no longer being a good quantum number.

The Breit-Rabi effect is observed by measuring the absorption spectra of the $6s^2\ ^1S_0 \leftrightarrow 6s6p\ ^1P_1$ transition in ^{171}Yb . The probe laser with wavelength 399 nm can be frequency-scanned using a fiber-EOM. Fig.6 shows the absorption spectra of three different branches in the $6s^2\ ^1S_0 \leftrightarrow 6s6p\ ^1P_1$ transition described in the main text. The red line in Fig.6(a) shows the absorption spectrum of the $^1S_0\ |1/2, \pm 1/2\rangle \leftrightarrow ^1P_1\ |\overline{3/2, \pm 1/2}\rangle$ transition detected using linearly polarized light along the z -axis. The blue line in Fig.6(a) shows the absorption spectrum of the $^1S_0\ |1/2, \pm 1/2\rangle \leftrightarrow ^1P_1\ |\overline{3/2, \pm 1/2}\rangle$ and $^1S_0\ |1/2, \pm 1/2\rangle \leftrightarrow ^1P_1\ |\overline{3/2, \pm 3/2}\rangle$ transition detected using linearly polarized light along the y -axis. In the presence of an electric field, due to the tensor Stark interaction, the degeneracy of the states $|\overline{3/2, \pm 1/2}\rangle$ and $|\overline{3/2, \pm 3/2}\rangle$ states of $6s6p\ ^1P_1$ is lifted, resulting in a double-peak structure in the absorption spectrum. By performing double-peak Lorentzian fitting, the centers of the transitions $^1S_0\ |1/2, \pm 1/2\rangle \leftrightarrow ^1P_1\ |\overline{3/2, \pm 1/2}\rangle$ and $^1S_0\ |1/2, \pm 1/2\rangle \leftrightarrow ^1P_1\ |\overline{3/2, \pm 3/2}\rangle$ can be obtained. Fig.6(b) shows the absorption spectrum of the $^1S_0\ |1/2, \pm 1/2\rangle \leftrightarrow ^1P_1\ |\overline{1/2, \pm 1/2}\rangle$ transition detected using linearly polarized light along the y -axis. The electric field is 19.96(3) kV/cm for the spectra measurement shown in Fig.6.

First Section introduces the eigenenergies and eigenstates of atoms that change when interacting with an external electric field. Besides this, the E1 transition rate from the ground state $|i\rangle = ^1S_0\ |1/2, 1/2\rangle$ to an energy eigenstate $|f\rangle = ^1P_1\ |\overline{F}, m_F\rangle$ is also affected by the electric field. The expression for the transition rate is given by

$$R_{i \rightarrow f} \propto |\langle i | -\mathbf{d} \cdot \boldsymbol{\epsilon} | f \rangle|^2 = |D_{if}|^2 \quad (13)$$

where the E1 transition matrix element is

$$D_{if} = \langle ^1S_0 \| \mathbf{d} \| ^1P_1 \rangle \sum_q \sum_{F'm'_F} (-1)^{I+F'+q} \epsilon_{-q} \sqrt{2(2F'+1)} \begin{pmatrix} 1/2 & 1 & F' \\ -1/2 & q & m'_F \end{pmatrix} \begin{Bmatrix} 1/2 & 1 & F' \\ 1 & 1/2 & 0 \end{Bmatrix} \langle F', m'_F | \overline{F}, m_F \rangle, \quad (14)$$

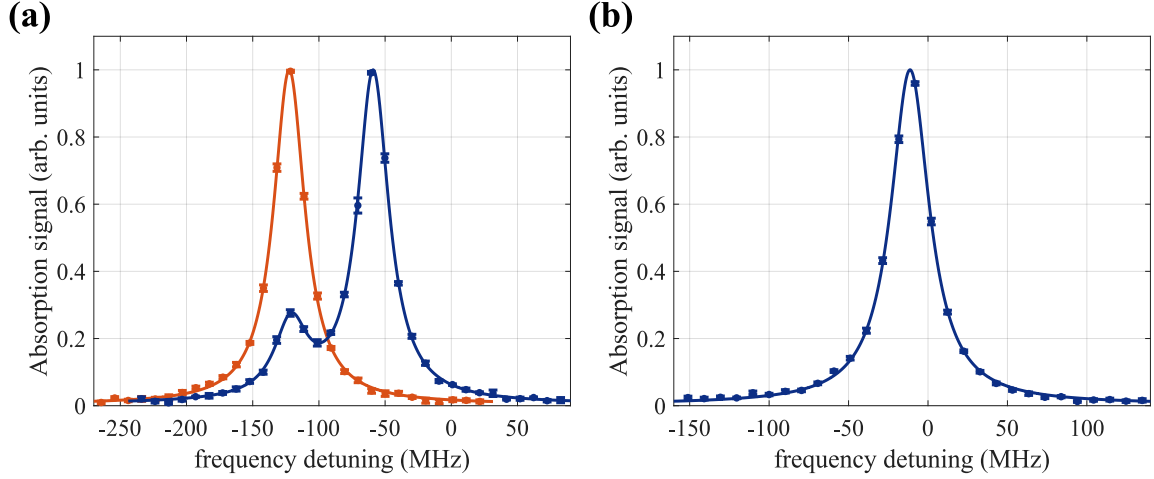


FIG. 6. Measurement of the $6s^2 \ ^1S_0 \rightarrow 6s6p \ ^1P_1$ transition spectrum of ^{171}Yb . (a) Spectrum of the $^1S_0 |1/2, m_F\rangle \rightarrow ^1P_1 |3/2, m_F\rangle$ transition at an electric field strength of $55.10(9)$ kV/cm. The orange spectrum is measured with linearly polarized light along the z-axis, corresponding to the $^1S_0 |1/2, \pm 1/2\rangle \rightarrow ^1P_1 |3/2, \pm 1/2\rangle$ transition. The blue spectrum is measured with linearly polarized light along the y-axis, and the blue solid line is the result of double-peak Lorentzian fitting. The peak on the right corresponds to the $^1S_0 |1/2, \pm 1/2\rangle \rightarrow ^1P_1 |3/2, \pm 3/2\rangle$ transition. (b) Spectrum of the $^1S_0 |1/2, \mp 1/2\rangle \rightarrow ^1P_1 |1/2, \pm 1/2\rangle$ transition measured with linearly polarized light along the y-axis at an electric field strength of $19.96(3)$ kV/cm.

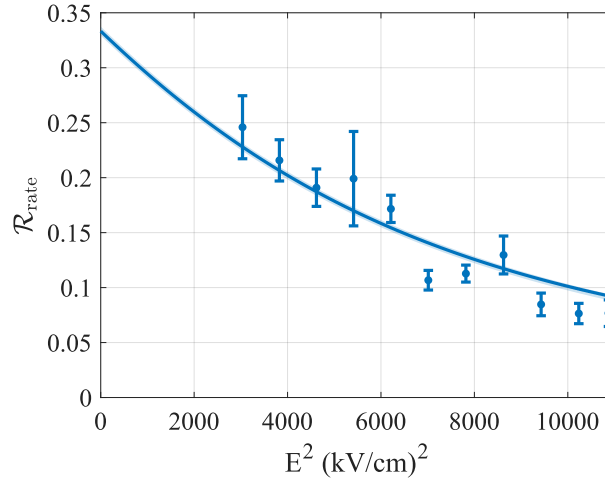


FIG. 7. $\mathcal{R}_{\text{rate}}$ vs. E^2 . The dependence of transition rates on the E field. $\mathcal{R}_{\text{rate}}$ of the vertical axis is the ratio between the transition rates of $^1S_0 |1/2, \pm 1/2\rangle \leftrightarrow ^1P_1 |3/2, \mp 1/2\rangle$ and $^1S_0 |1/2, \pm 1/2\rangle \leftrightarrow ^1P_1 |3/2, \pm 3/2\rangle$. The calculated results (solid line) agree with the data points. The error bars come from fitting to the signal shown in Fig. 6(a)

where $\langle ^1S_0 || \mathbf{d} || ^1P_1 \rangle$ is the reduced matrix element, and $\langle F', m'_F | \overline{F, m_F} \rangle$ is the projection of the energy eigenstate $|F', m'_F\rangle$ onto the angular momentum eigenstate $|F, m_F\rangle$. ϵ is the unit vector of the polarization of the light electric field, $\mathbf{d} = -|e|\mathbf{r}$ is the electric dipole operator, and the subscript q denotes the spherical tensor component.

Fig. 7 displays the ratio of transition rates ($\mathcal{R}_{\text{rate}}$) between transitions $^1S_0 |1/2, \pm 1/2\rangle \leftrightarrow ^1P_1 |3/2, \mp 1/2\rangle$ and $^1S_0 |1/2, \pm 1/2\rangle \leftrightarrow ^1P_1 |3/2, \pm 3/2\rangle$. The measured static data agree with calculated $\mathcal{R}_{\text{rate}}$ values (blue line). Using the electric Breit-Rabi formula, the differential static scalar polarizability ($\Delta\alpha_s$) and the static tensor polarizability (α_t) can be independently obtained from either the transition $^1S_0 |1/2, \pm 1/2\rangle \leftrightarrow ^1P_1 |3/2, \pm 1/2\rangle$ or $^1S_0 |1/2, \pm 1/2\rangle \leftrightarrow ^1P_1 |1/2, \mp 1/2\rangle$ as shown in the Table I. Those value are consistent with each other, and agree with the values obtained on even isotopes by Kawamura *et al.*[39]. To determine the hyperfine structure constant A_{hfs} , we scan the absorption spectra of $6s^2 \ ^1S_0 |1/2, m_F\rangle \rightarrow 6s6p \ ^1P_1 |1/2, m_F\rangle$ and $6s^2 \ ^1S_0 |1/2, m_F\rangle \rightarrow 6s6p \ ^1P_1 |3/2, m_F\rangle$ with the

TABLE I. Polarizability values.

Source	$\Delta\alpha_s$ (kHz/(kV/cm) ²)	α_t (kHz/(kV/cm) ²)
$^1S_0 1/2, \pm 1/2\rangle \leftrightarrow ^1P_1 3/2, \pm 1/2\rangle$	$57.79 \pm 0.17_{\text{stat}} \pm 0.19_{\text{syst}}$	$-19.44 \pm 0.11_{\text{stat}} \pm 0.06_{\text{syst}}$
$^1S_0 1/2, \pm 1/2\rangle \leftrightarrow ^1P_1 1/2, \mp 1/2\rangle$	$58.03 \pm 0.08_{\text{stat}} \pm 0.19_{\text{syst}}$	$-19.22 \pm 0.13_{\text{stat}} \pm 0.06_{\text{syst}}$
Previous works[39, 40]	59.12(67)	-19.47(17), -14.3(1.4)

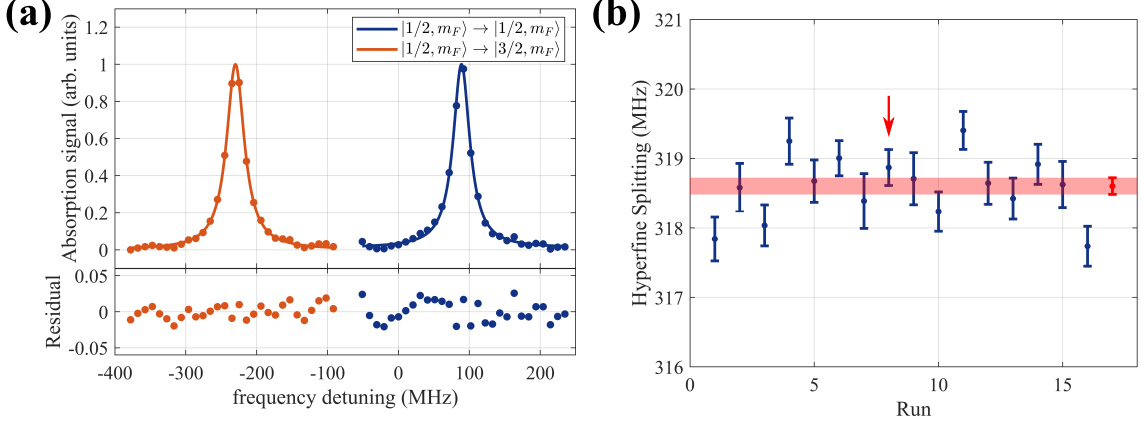


FIG. 8. Hyperfine structure constant measurement. (a) Spectra obtained in a single measurement. The orange line represents the transition $6s^2\ ^1S_0|1/2, m_F\rangle \rightarrow 6s6p\ ^1P_1|3/2, m_F\rangle$, with the fitted resonance and linewidth at -229.96(14) MHz and 29 MHz, respectively. The blue line represents the transition $6s^2\ ^1S_0|1/2, m_F\rangle \rightarrow 6s6p\ ^1P_1|1/2, m_F\rangle$, with the resonance and linewidth at 88.91(22) MHz and 29 MHz, respectively. The separation between the resonances is 318.87(26) MHz. (b) Results of 16 measurements. The red data point represents the weighted average of 16 measurements, yielding a value of 318.60(12) MHz, whose uncertainty is scaled by a factor of $\sqrt{\chi^2/\nu} = 1.6$. The spectrum in Fig. S4(a) corresponds to the data point marked by the red arrow in S4(b).

electric field turned off (Fig. 8(a)), and measure the frequency difference between the two resonances. By performing repeated measurements, we obtain a series of hyperfine splitting results (Fig. 8(b)). Hence, the value of the hyperfine structure constant A_{hfs} is determined to be -212.4(1) MHz.

ACKNOWLEDGMENTS

We would like to thank W.-T. Luo, J.-L. Zhang, L.-Y. Tang, Z.-C. Yan, W. Jiang, C.-L. Zou for helpful discussions. This work has been supported by the National Natural Science Foundation of China (NSFC) through Grants No. 12174371, and the Innovation Program for Quantum Science and Technology through Grant No. 2021ZD0303101.

-
- [1] P. ZEEMAN, The effect of magnetisation on the nature of light emitted by a substance, *Nature* **55**, 347 (1897).
 - [2] J. STARK, Observation of the separation of spectral lines by an electric field, *Nature* **92**, 401 (1913).
 - [3] G. Breit and I. I. Rabi, Measurement of nuclear spin, *Phys. Rev.* **38**, 2082 (1931).
 - [4] F. Paschen and E. Back, Normale und anomale zeemaneffekte, *Annalen der Physik* **344**, 897 (1912).
 - [5] T. D. Barrett, D. Stuart, O. Barter, and A. Kuhn, Nonlinear zeeman effects in the cavity-enhanced emission of polarised photons, *New Journal of Physics* **20**, 073030 (2018).
 - [6] M. Abe, R. Itoyama, Y. Komiya, T. Ito, T. Mashimo, and S. Tojo, Quantitative investigation of the zeeman and paschen-back effects of the hyperfine structure during the rubidium $5^2S_{1/2} \rightarrow 5^2D_{5/2}$ two-photon transition, *Phys. Rev. A* **99**, 053420 (2019).
 - [7] G. Bao, A. Wickenbrock, S. Rochester, W. Zhang, and D. Budker, Suppression of the nonlinear zeeman effect and heading error in earth-field-range alkali-vapor magnetometers, *Phys. Rev. Lett.* **120**, 033202 (2018).
 - [8] D. A. Steck, *Quantum and Atom Optics* (2019) pp. 349–355, available online at <http://steck.us/teaching>.
 - [9] J. R. P. Angel and P. G. H. Sandars, The hyperfine structure stark effect. i. theory, *Proceedings of the Royal Society of London. Series A, Mathematical and Physical Sciences* **305**, 125 (1968).

- [10] R. W. Schmieder, Matrix elements of the quadratic stark effect on atoms with hyperfine structure, *American Journal of Physics* **40**, 297 (1972).
- [11] M. Auzinsh, K. Bluss, R. Ferber, F. Gahbauer, A. Jarmola, M. S. Safronova, U. I. Safronova, and M. Tamanis, Level-crossing spectroscopy of the 7, 9, and $10D_{5/2}$ states of ^{133}Cs and validation of relativistic many-body calculations of the polarizabilities and hyperfine constants, *Phys. Rev. A* **75**, 022502 (2007).
- [12] M. Auzinsh, K. Blushs, R. Ferber, F. Gahbauer, A. Jarmola, and M. Tamanis, Electric field induced hyperfine level-crossings in (nd)cs at two-step laser excitation: Experiment and theory, *Optics Communications* **264**, 333 (2006).
- [13] R. C. Brown, N. B. Phillips, K. Beloy, W. F. McGrew, M. Schioppo, R. J. Fasano, G. Milani, X. Zhang, N. Hinkley, H. Leopardi, T. H. Yoon, D. Nicolodi, T. M. Fortier, and A. D. Ludlow, Hyperpolarizability and operational magic wavelength in an optical lattice clock, *Phys. Rev. Lett.* **119**, 253001 (2017).
- [14] A. C. Lee, J. Smith, P. Richerme, B. Neyenhuis, P. W. Hess, J. Zhang, and C. Monroe, Engineering large stark shifts for control of individual clock state qubits, *Phys. Rev. A* **94**, 042308 (2016).
- [15] N. Hinkley, J. A. Sherman, N. B. Phillips, M. Schioppo, N. D. Lemke, K. Beloy, M. Pizzocaro, C. W. Oates, and A. D. Ludlow, An atomic clock with 10^{-18} instability, *Science* **341**, 1215 (2013).
- [16] A. V. Gorshkov, A. M. Rey, A. J. Daley, M. M. Boyd, J. Ye, P. Zoller, and M. D. Lukin, Alkaline-earth-metal atoms as few-qubit quantum registers, *Phys. Rev. Lett.* **102**, 110503 (2009).
- [17] A. Jenkins, J. W. Lis, A. Senoo, W. F. McGrew, and A. M. Kaufman, Ytterbium nuclear-spin qubits in an optical tweezer array, *Phys. Rev. X* **12**, 021027 (2022).
- [18] M. A. Norcia, W. B. Cairncross, K. Barnes, P. Battaglini, A. Brown, M. O. Brown, K. Cassella, C.-A. Chen, R. Coxe, D. Crow, J. Epstein, C. Griger, A. M. W. Jones, H. Kim, J. M. Kindem, J. King, S. S. Kondov, K. Kotru, J. Lauigan, M. Li, M. Lu, E. Megidish, J. Marjanovic, M. McDonald, T. Mittiga, J. A. Muniz, S. Narayanaswami, C. Nishiguchi, R. Notermans, T. Paule, K. A. Pawlak, L. S. Peng, A. Ryou, A. Smull, D. Stack, M. Stone, A. Sucich, M. Urbanek, R. J. M. van de Veedonk, Z. Vendeiro, T. Wilkason, T.-Y. Wu, X. Xie, X. Zhang, and B. J. Bloom, Midcircuit qubit measurement and rearrangement in a ^{171}Yb atomic array, *Phys. Rev. X* **13**, 041034 (2023).
- [19] T. Fukuhara, Y. Takasu, M. Kumakura, and Y. Takahashi, Degenerate fermi gases of ytterbium, *Phys. Rev. Lett.* **98**, 030401 (2007).
- [20] M. Yamashita, S. Kato, A. Yamaguchi, S. Sugawa, T. Fukuhara, S. Uetake, and Y. Takahashi, Strongly interacting array of bose-einstein condensates trapped in a one-dimensional optical lattice, *Phys. Rev. A* **87**, 041604 (2013).
- [21] K. Beloy, N. Hinkley, N. B. Phillips, J. A. Sherman, M. Schioppo, J. Lehman, A. Feldman, L. M. Hanssen, C. W. Oates, and A. D. Ludlow, Atomic clock with 1×10^{-18} room-temperature blackbody stark uncertainty, *Phys. Rev. Lett.* **113**, 260801 (2014).
- [22] A. Aepli, K. Kim, W. Warfield, M. S. Safronova, and J. Ye, Clock with 8×10^{-19} systematic uncertainty, *Phys. Rev. Lett.* **133**, 023401 (2024).
- [23] M. Marinescu and L. You, Controlling atom-atom interaction at ultralow temperatures by dc electric fields, *Phys. Rev. Lett.* **81**, 4596 (1998).
- [24] Z. Li and R. V. Krems, Electric-field-induced feshbach resonances in ultracold alkali-metal mixtures, *Phys. Rev. A* **75**, 032709 (2007).
- [25] S. Omanakuttan, V. Buchemmavari, J. A. Gross, I. H. Deutsch, and M. Marvian, Fault-tolerant quantum computation using large spin-cat codes, *PRX Quantum* **5**, 020355 (2024).
- [26] M. Kleinert, M. E. Gold Dahl, and S. Bergeson, Measurement of the $\text{yb } i\ ^1s_0 - ^1p_1$ transition frequency at 399 nm using an optical frequency comb, *Phys. Rev. A* **94**, 052511 (2016).
- [27] Y. Takasu, K. Komori, K. Honda, M. Kumakura, T. Yabuzaki, and Y. Takahashi, Photoassociation spectroscopy of laser-cooled ytterbium atoms, *Phys. Rev. Lett.* **93**, 123202 (2004).
- [28] T. A. Zheng, Y. A. Yang, M. S. Safronova, U. I. Safronova, Z.-X. Xiong, T. Xia, and Z.-T. Lu, Magic wavelengths of the $\text{yb } (6s^2\ ^1s_0 - 6s6p\ ^3p_1)$ intercombination transition, *Phys. Rev. A* **102**, 062805 (2020).
- [29] J. Li and W. A. V. Wijngaarden, Stark shift measurement of the $(6s)^2\ ^1s_0$ to $(6s6p)^3p_1$ ytterbium transition, *Journal of Physics B: Atomic, Molecular and Optical Physics* **28**, 2559 (1995).
- [30] A. Vianello, Componentlibrary: A free vector graphics library for optics, <https://github.com/amv213/ComponentLibrary?tab=readme-ov-file> (2020).
- [31] M. Kawamura, W.-G. Jin, N. Kobayashi, S. Kanno, and T. Minowa, Stark effect of the $4f^{14}6s^2\ ^1s_0 - 4f^{14}6s6p\ ^1p_1$ transition in $\text{yb } i$, *Journal of the Physical Society of Japan* **82**, 045001 (2013).
- [32] M. Horbatsch and E. A. Hessels, Shifts from a distant neighboring resonance for a four-level atom, *Phys. Rev. A* **84**, 032508 (2011).
- [33] R. C. Brown, S. Wu, J. V. Porto, C. J. Sansonetti, C. E. Simien, S. M. Brewer, J. N. Tan, and J. D. Gillaspay, Quantum interference and light polarization effects in unresolvable atomic lines: Application to a precise measurement of the $^{6,7}\text{Li } D_2$ lines, *Phys. Rev. A* **87**, 032504 (2013).
- [34] T. Udem, L. Maisenbacher, A. Matveev, V. Andreev, A. Grinin, A. Beyer, N. Kolachevsky, R. Pohl, D. C. Yost, and T. W. Hänsch, Quantum interference line shifts of broad dipole-allowed transitions, *Annalen der Physik* **531**, 1900044 (2019).
- [35] T. P. Harty, D. T. C. Allcock, C. J. Ballance, L. Guidoni, H. A. Janacek, N. M. Linke, D. N. Stacey, and D. M. Lucas, High-fidelity preparation, gates, memory, and readout of a trapped-ion quantum bit, *Phys. Rev. Lett.* **113**, 220501 (2014).
- [36] J. J. Bollinger, J. D. Prestage, W. M. Itano, and D. J. Wineland, Laser-cooled-atomic frequency standard, *Phys. Rev. Lett.* **54**, 1000 (1985).
- [37] R. W. Schmieder, Matrix Elements of the Quadratic Stark Effect on Atoms with Hyperfine Structure, *American Journal of Physics* **40**, 297 (1972), https://pubs.aip.org/aapt/ajp/article-pdf/40/2/297/12152823/297.1_online.pdf.

- [38] G. Toh, D. Antypas, and D. S. Elliott, Measurement of the stark shift of the $6s^2S_{1/2} \rightarrow 7p^2P_J$ transitions in atomic cesium, [Phys. Rev. A **89**, 042512 \(2014\)](#).
- [39] M. Kawamura, W.-G. Jin, N. Kobayashi, S. Kanno, and T. Minowa, Stark effect of the $4f^{14}6s^2\ ^1s_0-4f^{14}6s6p\ ^1p_1$ transition in yb i, [Journal of the Physical Society of Japan **82**, 045001 \(2013\)](#).
- [40] R.-H. Rinkleff, Stark effect investigations of the $4f^{14}6s\ 6p^3p_1$ and $1p_1$ levels of ytterbium, [Zeitschrift für Physik A Atoms and Nuclei **296**, 101 \(1980\)](#).